# Growth of thin film organic crystals with strong nonlinearity for on-chip second-order nonlinear optics

A. Hermans,[1,2] R. Janneck,[3,4] C. Rolin,[3] S. Clemmen,[1,2,5] P. Heremans,[3,4] J. Genoe,[3,4] and R. Baets[1,2]

[1] Photonics Research Group, Ghent University-imec, Ghent, Belgium
[2] Center for Nano- and Biophotonics (NB-Photonics), Ghent University, Ghent, Belgium
[3] Large Area Electronics department (LAE), imec, Leuven, Belgium
[4] Department of Electrical Engineering (ESAT), KU Leuven, Leuven, Belgium
[5] Laboratoire d'Information Quantique, Université Libre de Bruxelles, Brussels, Belgium

*We have measured strong second-harmonic generation in N-benzyl-2-methyl-4-nitroaniline (BNA) thin films at a fundamental wavelength of 1550 nm. The second-order nonlinearity was determined to be (61 ± 10) pm/V, comparable to the benchmark nonlinear crystal LiNbO₃. The crystals are grown by cooling BNA from its melting point to room temperature in the presence of a temperature gradient. This gives rise to millimeter-sized crystals with thicknesses of several 100 nanometers. Our results are a first step towards the implementation of second-order nonlinear functionalities in silicon nitride photonic integrated circuits, where monolithically integrated strongly nonlinear crystals are lacking.*

## Introduction

The second-order optical nonlinearity (also known as the $2^{nd}$-order susceptibility $\chi^{(2)}$) of materials gives rise to interesting effects like second-harmonic generation (SHG), parametric down-conversion, and the Pockels effect [1]. These effects are put to use in various applications, including optical parametric oscillators (OPO's) [2], high-speed electro-optic (EO) modulators [3], and quantum light sources [4], all of them being commercialized at costs ranging from $1,000 to $100,000. Therefore, there is still a lot of room for improvement in terms of their cost, but also in terms of footprint and energy budget. We believe these improvements can be made by implementing $\chi^{(2)}$ based devices in an integrated photonics platform. While dedicated platforms are being developed based on AlGaAs or high index contrast LiNbO₃ [5-6], an ideal solution would consist in adding the $\chi^{(2)}$ nonlinearity to one of the existing CMOS-compatible platforms. Indeed, the use of existing CMOS infrastructure allows for high-volume, high-yield manufacturing at a low cost per chip. Next to the possibility of low-cost fabrication, the miniaturized photonic circuits with strong electric field confinement allow for more energy efficient $\chi^{(2)}$ based devices. However, the $\chi^{(2)}$ effect vanishes in centrosymmetric material systems [1]. Unfortunately, the materials typically available in silicon photonics technology, silicon (Si), amorphous silicon dioxide (SiO₂) and silicon nitride (SiN), possess the aforementioned property. Yet, there have been demonstrations of $\chi^{(2)}$ effects in Si [7] and SiN [8], but the precise origin remains uncertain and the overall nonlinearity modest. In recent years, substantial progress has been made in combining ferroelectric BTO [9-10] and PZT [3] with Si photonics to take advantage of their strong Pockels effect. On the other hand, very large $\chi^{(2)}$ nonlinearities have been reported for organic materials. Poled organic materials have been used successfully to demonstrate highly efficient Si-organic modulators [11]. However, these poled materials tend to lose their ordered structure over time. Organic crystals, like DAST [12] and BNA [13], do not require poling. For *N*-benzyl-2-methyl-4-nitroaniline,

or BNA, a nonlinearity of $\chi_{zzz} = (468 \pm 62)$ pm/V at a fundamental wavelength of 1064 nm has been reported in bulk crystals [13] (compared to $\chi_{zzz} = 54$ pm/V for LiNbO$_3$ [14], used in many applications). Also EO modulators have been demonstrated in Si slot waveguides filled with BNA [15-16]. BNA belongs to the orthorhombic crystal system, point group mm2 [15]. It is transparent in the ~500 nm to ~2 μm wavelength range [13]. The ability to grow these organic crystals in thin films over large areas would enable their integration in nanophotonic circuits, and consequently allow the realization of efficient integrated $\chi^{(2)}$ devices. Considering the large overlap in transparency windows between SiN and BNA, this platform is the natural choice for nonlinear wave mixing experiments.

Here we report on the growth of high $\chi^{(2)}$ millimeter-sized BNA crystals with thicknesses in the 200 to 600 nm range. The fabrication process is outlined, along with characterization through x-ray diffraction (XRD) and SHG measurements.

## Crystal growth

The first step in the fabrication process is the drop casting of a BNA in toluene solution on an oxidized Si substrate. A glass cover is placed on top to avoid dewetting in subsequent steps. Next, BNA is molten by heating up the sample on a hotplate. Finally, the sample is cooled down slowly in the presence of a temperature gradient to promote the formation of large crystals. We use 2 cm × 2 cm glass covers and oxidized Si substrates (100 nm SiO$_2$). Before processing the substrates are cleaned in an ultrasonic bath using soap, DI water, acetone, and IPA, followed by a 15 minutes UV-O$_3$ treatment. BNA was purchased in powder form from MolPort. We dissolve the powder in toluene. For the drop casting we use 100 μl of 0.4 wt% BNA in toluene solution. After the solvent has evaporated, the glass cover is placed on top. For the crystallization, the sample is placed on a Unitemp RSS-450-110 hotplate whose temperature profile over time can be programmed. When placing the sample on the hotplate, we pay attention to position the sample such that it is extending from the side of the hotplate (by several millimeters). This creates a small temperature gradient. The sample is heated up to 105°C (BNA's melting point [16]) in 5 minutes, after which it stays at 105°C for 1 minute. Finally, it is cooled down to room temperature at a rate of -0.1°C/minute. Before characterization the glass cover is removed.

## Characterization methods

For visual inspection of our samples an Olympus DSX 500 microscope is used. We utilize the polarized light option since it gives good contrast between different crystal orientations for anisotropic materials. The Veeco Dektak 150 surface profiler is used to determine the thin film thickness. X-ray analysis is done with a Bruker D8 Discover system utilizing Cu Kα radiation. The SHG measurements are performed on a home-built setup (Fig. 1). The laser source is a Calmar FPL-03CCFPM femtosecond fiber laser with a wavelength of 1550 nm and a pulse duration of 100 fs. The laser beam is collimated and sent through a polarizing beamsplitter cube (PBSC) to obtain linearly polarized light. Next, the beam passes through a half-wave plate to alter the polarization direction. Afterwards, the laser light is focused onto the sample with a parabolic mirror and a 2$^{nd}$ parabolic mirror directs the light to the detector (IDQ ID 120). In front and behind the sample there are a longpass and shortpass filter, to filter out light at the second-harmonic (SH) wavelength that is not generated in the sample and to filter out the laser light, respectively. In front of the detector there is also a PBSC, to select the

polarization of interest, a bandpass filter, to filter out all light not at the SH wavelength, and a lens to focus the light onto the detector. The setup is calibrated with a BBO crystal. To fit our data, the model described in [17] has been implemented in MATLAB.
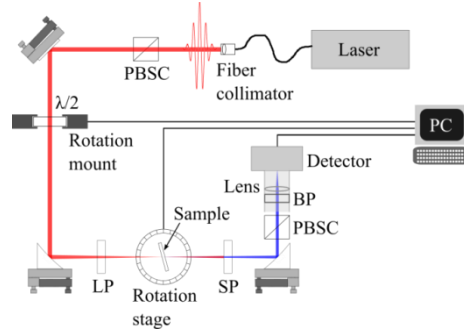


Fig. 1. Setup for SHG measurements. PBSC = polarizing beamsplitter cube, λ/2 = half-wave plate, LP = longpass filter, SP = shortpass filter, BP = bandpass filter.

## Results and discussion

Millimeter-sized BNA crystals can be seen on the microscopy image in Fig. 2a. The black regions are gaps or cracks. Fig. 2b shows a surface profile measured over one of these gaps, giving us an estimate of the film thickness. The drop casting technique results in thicknesses varying from 200 to 600 nm, though locally the variations are small as can be seen from the surface profile. XRD $\theta$-$2\theta$ scans show higher-order diffraction peaks corresponding to the (010) plane (Fig. 3a).



| (a) | (b) |
|---|---|
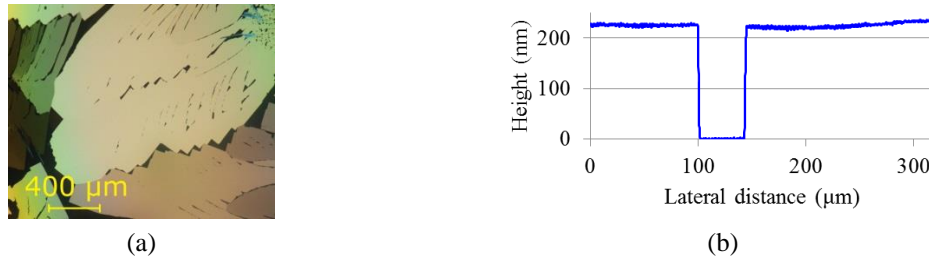
Fig. 2. (a) Polarized light microscopy image. (b) Surface profile of BNA crystals.



| (a) | (b) |
|---|---|

Fig. 3. (a) XRD $\theta$-$2\theta$ scan of BNA. (b) Measurement and fit of SH power for normal incidence and varying input polarization (0° corresponds to s-polarized light). The PBSC in front of the detector is oriented such that p-polarized SH waves (polarization angle of 90°) are transmitted.

Knowing the crystal orientation, thickness, and refractive index [13], we can determine the nonlinearity in SHG measurements (Fig. 3b). The SH power is measured as a function of polarization angle at normal incidence. The position of the maximum depends on the in-plane crystal orientation. Fitting gives a nonlinearity of $\chi_{zzz} = (61 \pm 10)$ pm/V (error due to thickness uncertainty; result is an average of 6 measurements spread over 3 samples). For bulk crystals a value of $(468 \pm 62)$ pm/V at 1064 nm is reported. Taking into account dispersion, this corresponds to ~314 pm/V at 1550 nm [18]. Our smaller value can be related to the crystal quality.

In conclusion, we demonstrated large area growth of BNA thin film organic crystals with a large $\chi^{(2)}$ nonlinearity. These results are a first step towards the implementation of $\chi^{(2)}$ functionalities in SiN photonic integrated circuits.

## References

[1] G. New, Introduction to Nonlinear Optics, Cambridge University Press, 2011.

[2] J. A. Giordmaine and R. C. Miller, "Tunable coherent parametric oscillation in LiNbO$_3$ at optical frequencies," Phys. Rev. Lett., vol. 14, 973, 1965.

[3] K. Alexander, J. P. George, J. Verbist, K. Neyts, B. Kuyken, D. Van Thourhout, and J. Beeckman, "Nanophotonic Pockels modulators on a a silicon nitride platform," Nat. Commun., vol. 9, 3444, 2018.

[4] P. G. Kwiat, K. Mattle, H. Weinfurter, A. Zeilinger, A. V. Sergienko, and Y. Shih, "New high-intensity source of polarization-entangled photon pairs," Phys. Rev. Lett., vol. 75, 4337, 1995.

[5] L. Ottaviano, M. Pu, E. Semenova, and K. Yvind, "Low-loss high-confinement waveguides and microring resonators in AlGaAs-on-insulator," Opt. Lett., vol. 41, 3996, 2016.

[6] C. Wang, M. Zhang, X. Chen, M. Bertrand, A. Shams-Ansari, S. Chandrasekhar, P. Winzer, and M. Lončar, "Integrated lithium niobate electro-optic modulators operating at CMOS-compatible voltages," Nature, vol. 562, 101, 2018.

[7] R. S. Jacobsen, K. N. Andersen, P. I. Borel, J. Fage-Pedersen, L. H. Frandsen, O. Hansen, M. Kristensen, A. V. Lavrinenko, G. Moulin, H. Ou, C. Peucheret, B. Zsigri, and A. Bjarklev, "Strained silicon as a new electro-optic material," Nature, vol. 441, 199, 2006.

[8] T. Ning, H. Pietarinen, O. Hyvärinen. J. Simonen, G. Genty, and M. Kauranen, "Strong second-harmonic generation in silicon nitride films," Appl. Phys. Lett., vol. 100, 161902, 2012.

[9] C. Xiong, W. H. P. Pernice, J. H. Ngai, J. W. Reiner, D. Kumah, F. J. Walker, C. H. Ahn, and H. X. Tang, "Active silicon integrated nanophotonics: ferroelectric BaTiO$_3$," Nano Lett., vol. 14, 1419, 2014.

[10] F. Eltes, D. Caimi, F. Fallegger, M. Sousa, E. O'Conner, M. D. Rossell, B. Offrein, J. Fompeyrine, and S. Abel, "Low-loss BaTiO$_3$-Si waveguides for nonlinear integrated photonics," ACS Photonics, vol. 3, 1698, 2016.

[11] C. Koos, J. Leuthold, W. Freude, M. Kohl, L. Dalton, W. Bogaerts, A. L. Giesecke, M. Lauermann, A. Melikyan, S. Koeber, S. Wolf, C. Weimann, S. Muehlbrandt, K. Koehnle, J. Pfeifle, W. Hartmann, Y. Kutuvantavida, S. Ummethala, R. Palmer, D. Korn, L. Alloati, P. C. Schindler, D. L. Elder, T. Wahlbrink, and J. Bolten, "Silicon-organic hybrid (SOH) and plasmonic-organic hybrid (POH) integration," J. Light. Technol., vol. 34, 256, 2016.

[12] M. Jazbinsek, L. Mutter, and P. Günter, "Photonic applications with the organic nonlinear optical crystal DAST," IEEE J. Sel. Top. Quantum Electron., vol. 14, 1298, 2008.

[13] M. Fujiwara, M. Maruyama, M. Sugisaki, H. Takahashi, S. Aoshima, R. J. Cogdell, and H. Hashimoto, "Determination of the *d*-tensor components of a single crystal of *N*-benzyl-2-methyl-4-nitroaniline," Jpn. J. Appl. Phys., vol. 46, 1528, 2007.

[14] D. A. Roberts, "Simplified characterization of uniaxial and biaxial nonlinear optical crystals: a plea for standardization of nomenclature and conventions," IEEE J. Quantum Electron., vol. 28, 2057, 1992.

[15] H. Figi, D. H. Bale, A. Szep, L. R. Dalton, and A. Chen, "Electro-optic modulation in horizontally slotted silicon/organic crystal hybrid devices," J. Opt. Soc. Am. B, vol. 28, 2291, 2011.

[16] D. Korn, M. Jazbinsek, R. Palmer, M. Baier, L. Alloati, H. Yu, W. Bogaerts, G. Lepage, P. Verheyen, P. Absil, P. Guenter, C. Koos, W. Freude, and J. Leuthold, "Electro-optic organic crystal silicon high-speed modulator," IEEE Photon. J., vol. 6, 2700109, 2014.

[17] D. S. Bethune, "Optical harmonic generation and mixing in multilayer media: extension of optical transfer matrix approach to include anisotropic materials," J. Opt. Soc. Am. B, vol. 8, 367, 1991.

[18] R. C. Miller, "Optical second harmonic generation in piezoelectric crystals," Appl. Phys. Lett., vol. 5, 17, 1964.